

highly purified HSC fraction identifies mitochondrial clearance by induction of mitophagosome formation as a key mechanism in maintaining stemness.

REFERENCES AND NOTES

1. K. Ito, T. Suda, *Nat. Rev. Mol. Cell Biol.* **15**, 243–256 (2014).
2. N. Shyh-Chang, G. Q. Daley, L. C. Cantley, *Development* **140**, 2535–2547 (2013).
3. K. Ito et al., *Nat. Med.* **18**, 1350–1358 (2012).
4. M. Mohrin et al., *Science* **347**, 1374–1377 (2015).
5. M. R. Warr et al., *Nature* **494**, 323–327 (2013).
6. M. Mortensen et al., *Proc. Natl. Acad. Sci. U.S.A.* **107**, 832–837 (2010).
7. L. Galluzzi, F. Pietrocola, B. Levine, G. Kroemer, *Cell* **159**, 1263–1276 (2014).
8. P. Katajisto et al., *Science* **348**, 340–343 (2015).
9. F. Arai et al., *Cell* **118**, 149–161 (2004).
10. M. Acar et al., *Nature* **526**, 126–130 (2015).
11. Y. Kunisaki et al., *Nature* **502**, 637–643 (2013).
12. W. H. Kunau, V. Dommès, H. Schulz, *Prog. Lipid Res.* **34**, 267–342 (1995).
13. R. Yamamoto et al., *Cell* **154**, 1112–1126 (2013).

ACKNOWLEDGMENTS

We thank all members of the Ito lab and Einstein Stem Cell Institute for their comments on HSC self-renewal and M. Wolfgang, A. Carracedo, H. You, and the Einstein Flow Cytometry and Analytical Imaging core facilities (grant P30CA013330) for help and materials. This work was supported by NIH (grants R01DK98263 and R01DK100689 to Ke.I.) and NYSTEM (New York State Stem Cell Science single-cell-core, grant C029154 to Ke.I.), Harvard Stem Cell

Institute (to C.P.L.), NIH and Ellison Medical Foundation (to R.S.), NIH and Leukemia Lymphoma Society (to P.S.F.), and Japan Society for the Promotion of Science (to T.S.). We declare no competing financial interests.

SUPPLEMENTARY MATERIALS

www.sciencemag.org/content/354/6316/1156/suppl/DC1
Materials and Methods
Supplementary Text
Figs. S1 to S14
References (14–59)
Movies S1 and S2

26 February 2016; accepted 4 October 2016
Published online 13 October 2016
10.1126/science.aaf5530

T CELL EXHAUSTION

Epigenetic stability of exhausted T cells limits durability of reinvigoration by PD-1 blockade

Kristen E. Pauken,¹ Morgan A. Sammons,² Pamela M. Odorizzi,¹ Sasikanth Manne,¹ Jernej Godec,^{3,4} Omar Khan,¹ Adam M. Drake,² Zeyu Chen,¹ Debattama R. Sen,³ Makoto Kurachi,¹ R. Anthony Barnitz,³ Caroline Bartman,¹ Bertram Bengsch,¹ Alexander C. Huang,⁵ Jason M. Schenkel,⁶ Golnaz Vahedi,⁷ W. Nicholas Haining,^{3,8,9} Shelley L. Berger,² E. John Wherry^{1*}

Blocking Programmed Death-1 (PD-1) can reinvigorate exhausted CD8 T cells (T_{EX}) and improve control of chronic infections and cancer. However, whether blocking PD-1 can reprogram T_{EX} into durable memory T cells (T_{MEM}) is unclear. We found that reinvigoration of T_{EX} in mice by PD-L1 blockade caused minimal memory development. After blockade, reinvigorated T_{EX} became reexhausted if antigen concentration remained high and failed to become T_{MEM} upon antigen clearance. T_{EX} acquired an epigenetic profile distinct from that of effector T cells (T_{EFF}) and T_{MEM} cells that was minimally remodeled after PD-L1 blockade. This finding suggests that T_{EX} are a distinct lineage of CD8 T cells. Nevertheless, PD-1 pathway blockade resulted in transcriptional rewiring and reengagement of effector circuitry in the T_{EX} epigenetic landscape. These data indicate that epigenetic fate inflexibility may limit current immunotherapies.

Persisting antigenic stimulation during chronic infections and cancer can result in T cell exhaustion, a state of impaired effector functions, high expression of inhibitory receptors including Programmed Death-1 (PD-1, or CD279), transcriptional reprogramming, and defective immune memory (1). Collectively, these

properties prevent optimal control of persisting pathogens and tumors. Blocking the PD-1:PD-L1 pathway can reinvigorate exhausted CD8 T cells (T_{EX}), improving effector functions and enhancing viral and tumor control (2). Recently developed inhibitors of the PD-1 and cytotoxic T lymphocyte-associated protein 4 (CTLA-4) pathways represent a new paradigm in cancer treatment (2–4). Although promising, the majority of patients fail to develop durable responses, and most eventually progress (2–4). Thus, it is unclear whether blocking PD-1 can promote long-lasting improvements and immunological memory development in T_{EX} .

To address this question, we analyzed the cellular, transcriptional, and epigenetic changes associated with PD-1 pathway blockade using the mouse model of chronic lymphocytic choriomeningitis virus (LCMV) infection (fig. S1, A to C) (5, 6). After treatment with antibodies against PD-L1 (anti-PD-L1), 1080 genes were up-regulated and 1686 genes were down-regulated [$P < 0.05$, \log_2 fold change (LFC) ≥ 0.2] (Fig. 1A, fig. S1D,

and table S1). Previous studies identified transcriptional (7) or cellular (8, 9) changes in metabolic pathways after PD-1 pathway blockade. Indeed, several metabolic genes were altered following PD-L1 blockade (table S1). Gene Set Enrichment Analysis (GSEA), however, identified more prominent changes in cell division pathways (Fig. 1B and table S2) (5, 10). In addition, many effector-related genes were biased toward the anti-PD-L1 group (Fig. 1, C and D, and table S3). Other genes of interest included *Cxcl9*, *Il1r2*, and *Il7r* (up-regulated) and *Klra9*, *Tnfrsf9*, and *Cd200r2* (down-regulated) (fig. S1D and table S1). Using leading-edge metagene (LEM) analysis (11), we identified two metagenes in anti-PD-L1-treated T_{EX} compared to control T_{EX} ; one corresponding to leukocyte activation and one to cell cycle (Fig. 1E; fig. S1, E and F; and table S4). The anti-PD-L1-treated T_{EX} metagenes displayed some overlap with effector T cells (T_{EFF}), largely driven by cell cycle pathways, but minimal overlap with T_{MEM} (Fig. 1E and table S4), suggesting limited acquisition of memory potential upon T_{EX} reinvigoration.

PD-1 pathway blockade can reactivate functions in T_{EX} , but whether reinvigoration is sustained is unclear. There was a robust reinvigoration of T_{EX} , as expected (Fig. 1, F and G, and figs. S1, A and B, and S2) (5), and expansion peaked ~3 weeks after initiation of blockade. By 8 to 11 weeks after treatment, however, this reinvigoration was lost, and the quantity, proliferation, effector function, and inhibitory receptor expression of LCMV-specific CD8 T cells in the anti-PD-L1-treated mice were comparable to those in control-treated mice (Fig. 1, F to H, and figs. S2 to S4). Moreover, although anti-PD-L1 treatment reduced viral load immediately after treatment, 4 months later, viral load was similar to that in control-treated mice (Fig. 1I). Lastly, 18 to 29 weeks after cessation of blockade, the transcriptional profiles of control- and anti-PD-L1-treated groups were similar (Fig. 1J, figs. S5 and S6, and tables S5 and S6). Collectively, these data indicate that when antigen concentration remains high, T_{EX} that were reinvigorated by PD-1 pathway blockade become “reexhausted.”

One possible reason the effects of PD-L1 blockade were not sustained is that the infection persisted. We hypothesized that if the infection were cleared, anti-PD-L1 might induce differentiation into T_{MEM} .

¹Department of Microbiology and Institute for Immunology, Perelman School of Medicine, University of Pennsylvania, Philadelphia, PA, USA. ²Departments of Cell and Developmental Biology, Genetics, and Biology, Penn Epigenetics Program, University of Pennsylvania, Philadelphia, PA, USA. ³Department of Pediatric Oncology, Dana-Farber Cancer Institute, Boston, MA, USA. ⁴Department of Microbiology and Immunobiology, Harvard Medical School, Boston, MA, USA. ⁵Department of Medicine and Institute for Immunology, Perelman School of Medicine, University of Pennsylvania, Philadelphia, PA, USA. ⁶Department of Microbiology and Immunology, University of Minnesota, Minneapolis, MN, USA. ⁷Department of Genetics and Institute for Immunology, University of Pennsylvania, Philadelphia, PA, USA. ⁸Broad Institute of MIT and Harvard, Cambridge, MA, USA. ⁹Division of Hematology/Oncology, Children’s Hospital, Harvard Medical School, Boston, MA, USA. *Corresponding author. Email: wherry@mail.med.upenn.edu

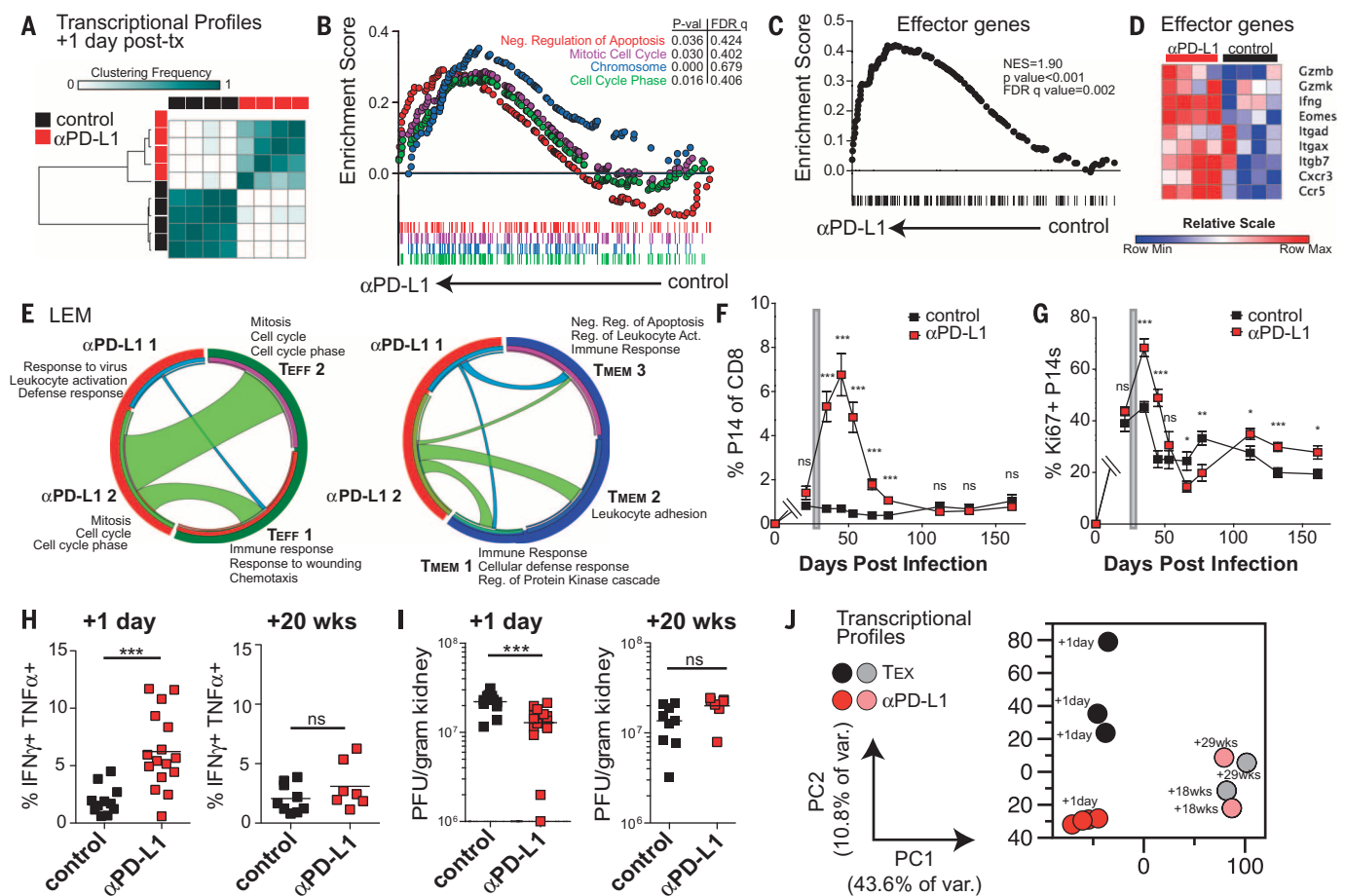


Fig. 1. Anti-PD-L1 induces an effector-like transcriptional program in T_{EX} cells that is not sustained after cessation of treatment. (A) Consensus hierarchical clustering by 1-Pearson correlation from the microarray on control- or anti-PD-L1-treated T_{EX} . (B) GSEA of representative Gene Ontology (GO) terms. (C) GSEA of effector genes. (D) Row-normalized heat map of effector-associated genes. (E) Circos plots showing overlap in metagenes identified in anti-PD-L1-treated T_{EX} compared to metagenes in T_{EFF} (left) and T_{MEM} cells (right). Ribbons connecting areas of the Circos plots indicate shared genes between groups. The microarray includes four independent experiments with 10 to 12 mice per group per experiment. (F) Frequency of LCMV GP33-specific T cell receptor transgenic “P14” cells among CD8 T cells and (G) Ki67⁺ P14 cells in the peripheral blood. Gray bar indicates antibody treatment period. Error bars represent SEM.

(H) Quantification of IFN γ ⁺ TNF α ⁺ P14 cells. (I) Viral load in the kidney. Data in (F) and (G) are one representative experiment. In (H) and (I), the ⁺¹ day time point is combined from two representative experiments, and the ⁺²⁰ week time point is from one representative experiment. Data in (F) to (I) are representative of at least two independent experiments with at least four mice per group per experiment. (J) Principle-component analysis of RNA sequencing (RNA-seq), percentage of variance (% of var.) indicated. The RNA-seq was performed on two to four independent experiments with 5 to 13 mice per group as indicated in the supplementary methods. Each dot represents an independent replicate. Asterisks indicate statistical significance determined by unpaired *t* tests between groups (**P* < 0.05, ***P* < 0.01, and ****P* < 0.001). ns, not significant.

To test this idea, we transferred equal numbers of control T_{EX} , anti-PD-L1-treated T_{EX} , or T_{MEM} into antigen-free mice and monitored persistence (fig. S7A). Consistent with previous studies (12, 13), T_{EX} survived poorly in antigen-free recipients compared to functional T_{MEM} (Fig. 2, A and B). There was a trend toward anti-PD-L1-treated T_{EX} persisting somewhat longer, though survival was poor compared to T_{MEM} (Fig. 2, A and B). We next investigated potential mechanisms for this trend. After PD-1 pathway blockade, the number of interleukin-7 (IL-7) receptor transcripts (*Il7r*; CD127) increased significantly (fig. S1D and table S1). There was also a modest increase in CD127 protein abundance on a subset of T_{EX} after anti-PD-L1 treatment (Fig. 2, C to E). Upon stimulation with IL-7, anti-PD-L1-treated T_{EX} also showed more phospho-STAT5 (signal transducer

and activator of transcription 5) compared to control-treated T_{EX} (Fig. 2F and fig. S7B). By contrast, expression of the IL-15 receptor subunit CD122 and responsiveness to IL-15 in vitro were not substantially altered (Fig. 2, C and F, and fig. S7B). These data suggest that anti-PD-L1 treatment may augment activity of the memory-biased IL-7R pathway.

Treatment with IL-7 starting in the effector phase can prevent development of exhaustion (14, 15). However, later in chronic infection, T_{EX} respond poorly to IL-7 (12, 13). Because anti-PD-L1 improved IL-7R signaling, we tested whether combined treatment had additional benefit (fig. S7C). Indeed, although other aspects of the response were less affected, treatment with IL-7 and anti-PD-L1, but not IL-7 alone, resulted in more antigen-specific CD8 T cells and improved coproduction

of interferon- γ (IFN- γ) and tumor necrosis factor- α (TNF- α) (Fig. 2, G to H, and fig. S7, D to H). Thus, it may be possible to exploit pathways up-regulated by PD-L1 blockade, including IL-7R, to improve checkpoint blockade.

We next examined whether PD-1 pathway blockade could restore recall potential upon reinfection, a defining property of T_{MEM} . Equal numbers of D^bGP33⁺ CD8 T_{EX} , anti-PD-L1-treated T_{EX} , or T_{MEM} were transferred into antigen-free mice, rested, and then rechallenged with *Listeria monocytogenes* expressing GP33-41. T_{MEM} robustly expanded and efficiently produced IFN- γ (Fig. 3, A to D). By contrast, both control- and anti-PD-L1-treated T_{EX} mounted poor responses to *Listeria*-GP33 challenge, and reinvigorated T_{EX} were as defective as control T_{EX} in these key properties (Fig. 3, A to D).

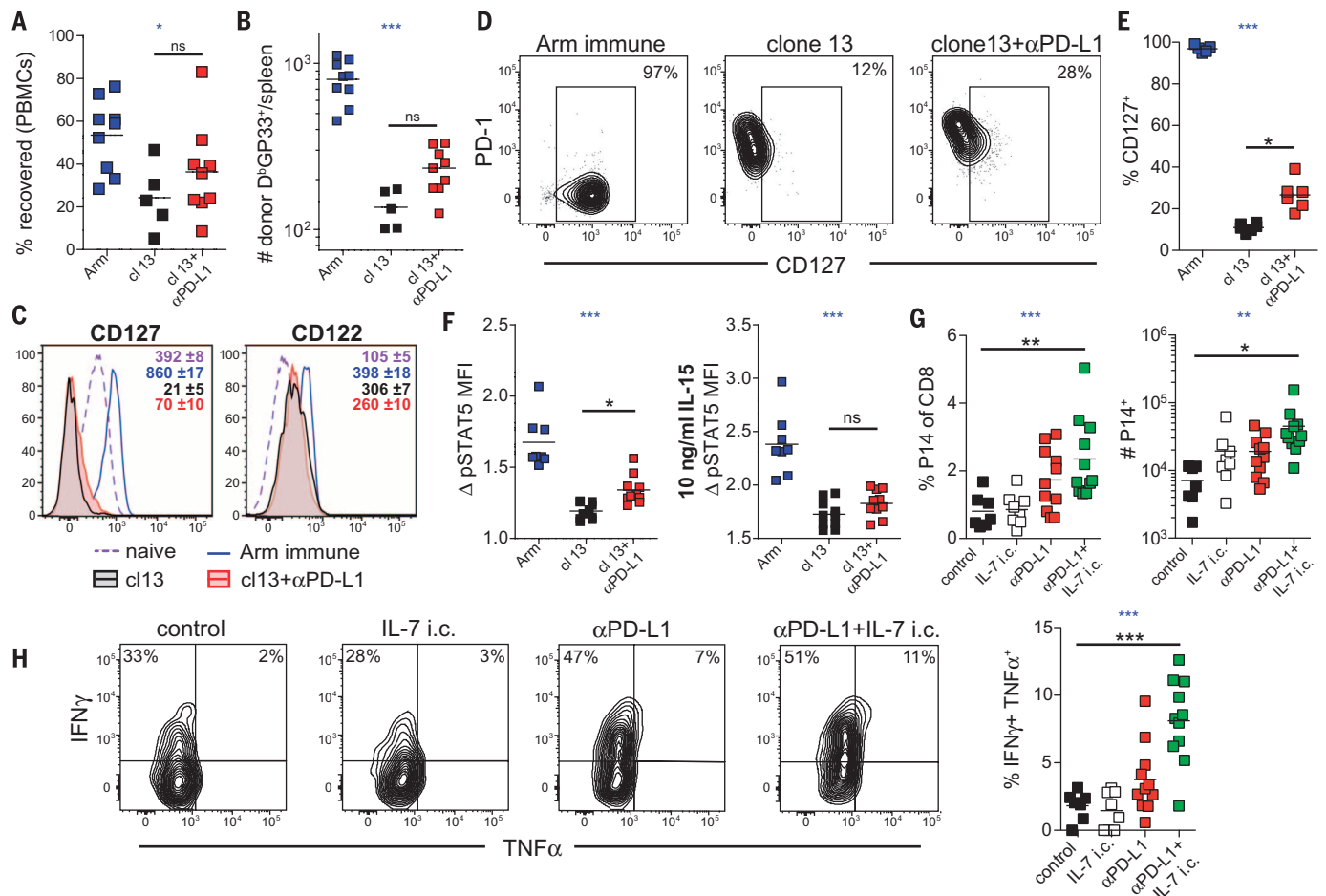


Fig. 2. PD-1 pathway blockade moderately improves antigen-independent persistence and IL-7 signaling in T_{EX} . (A) Number of D^bGP33^+ donor CD8 T cells per million peripheral blood mononuclear cells (PBMCs) at day 27 (compared to day 1) after transfer and (B) number recovered from the spleen. (C) Histograms of CD127 and CD122 expression on T_{EX} P14 cells (day 35 after clone 13) compared to T_{MEM} P14 cells or bulk $CD44^{lo}CD62L^+$ T_N cells [day 167 after LCMV strain Armstrong (Arm)]. Values indicate average geometric mean fluorescence intensity (MFI) and SEM. (D) Contour plots of PD-1 versus CD127 from mice in (C). (E) Quantification of (D). Data in (A) to (E) are representative of at least two independent experiments with at least four mice per group. (F) Quantification of

phospho-STAT5 induction by P14 cells at day 39 after infection after ex vivo stimulation with IL-7 or IL-15 for 30 min. Values indicate fold change over unstimulated controls. (G) Frequency (of $CD8^+$, left) and number (right) of P14 cells in the spleen after 2 weeks of treatment. (H) Plots (left) and quantification (right) of $IFN\gamma^+ TNF\alpha^+$ P14 cells from (G) after ex vivo peptide stimulation. Data in (F) to (H) are combined from two independent experiments with at least four mice per group. Asterisks indicate statistical significance (* $P < 0.05$, ** $P < 0.01$, and *** $P < 0.001$) determined as described in the supplementary materials. Blue asterisks indicate analysis of variance (ANOVA) P values; black asterisks indicate post-test P values.

After antigen withdrawal, T_{EX} and anti-PD-L1-treated T_{EX} failed to down-regulate PD-1 (Fig. 3E), consistent with *Pdcd1* locus DNA methylation and long-term expression of PD-1 (16–18). T_{EX} also have lower global diacetylated histone H3 (19), but how this relates to differentiation is unclear. We hypothesized that the genome-wide epigenetic landscape of T_{EX} may contribute to the lack of durable improvements after PD-1 pathway blockade. Thus, we performed global chromatin landscape mapping using assay for transposase-accessible chromatin with high-throughput sequencing (ATAC-seq) (20) (fig. S8). The majority of open chromatin regions (OCRs) identified were in intergenic regions (33.3 to 43.3%) or introns (43.4 to 48.5%) (fig. S9A), as expected (21). T_{EFF} , T_{MEM} , and T_{EX} showed substantial chromatin remodeling compared to T_N (Fig. 3F and fig. S9, B and C), and genes with transcriptional start sites

(TSS) within 20 kb of OCRs tended to be more highly expressed (fig. S10). OCRs at specific genes illustrated distinct patterns for T_{EFF} , T_{MEM} , and T_{EX} . For example, T_{EX} lacked several OCRs present in the *Ifng* locus in T_{EFF} and T_{MEM} (Fig. 3G, blue boxes). Similarly, for *Pdcd1*, T_{EX} -specific OCRs were identified in the “B” and “C” regions (Fig. 3G, black box) (9, 22, 23) and a previously unidentified OCR ~23 kb from the TSS (Fig. 3G, red box). Global hierarchical clustering and cocluster analysis showed that T_{EFF} and T_{MEM} were more similar to each other than to T_{EX} and that T_{EX} had a distinct global epigenetic landscape (Fig. 3, H to J, and figs. S11 to S13). These data suggest that T_{EX} may represent a distinct lineage of CD8 T cells.

Two subsets of T_{EX} have been defined based on expression of Eomes, T-bet, and PD-1 (24, 25), and additional heterogeneity has recently been described (26–28). The $T\text{-bet}^{hi}Eomes^{lo}PD-1^{int}$ sub-

set can be reinvigorated by PD-1 pathway blockade, whereas the $Eomes^{hi}PD-1^{hi}$ subset is more terminal and responds poorly to blocking PD-1 (24, 25). In this study, T_{EX} were ~80% $Eomes^{hi}$ and ~20% $T\text{-bet}^{hi}$, and this distribution changed minimally upon anti-PD-L1 treatment (fig. S14, A to C). The transcriptional and epigenetic profiles of T_{EX} and anti-PD-L1-treated T_{EX} were significantly enriched for genes from the $Eomes^{hi}$ subset (fig. S14, D and E) (29). However, there was also a trend toward enrichment of genes from the $PD-1^{int}Tbet^{hi}$ T_{EX} subset in the anti-PD-L1-treated group (fig. S14, F and G), perhaps reflecting recent conversion of $Tbet^{hi}$ cells into $Eomes^{hi}$ cells or additional heterogeneity.

We next examined the ability of PD-1 pathway blockade to reprogram the epigenetic landscape of T_{EX} . Hierarchical clustering, co-clustering, and principle-component analysis showed considerable

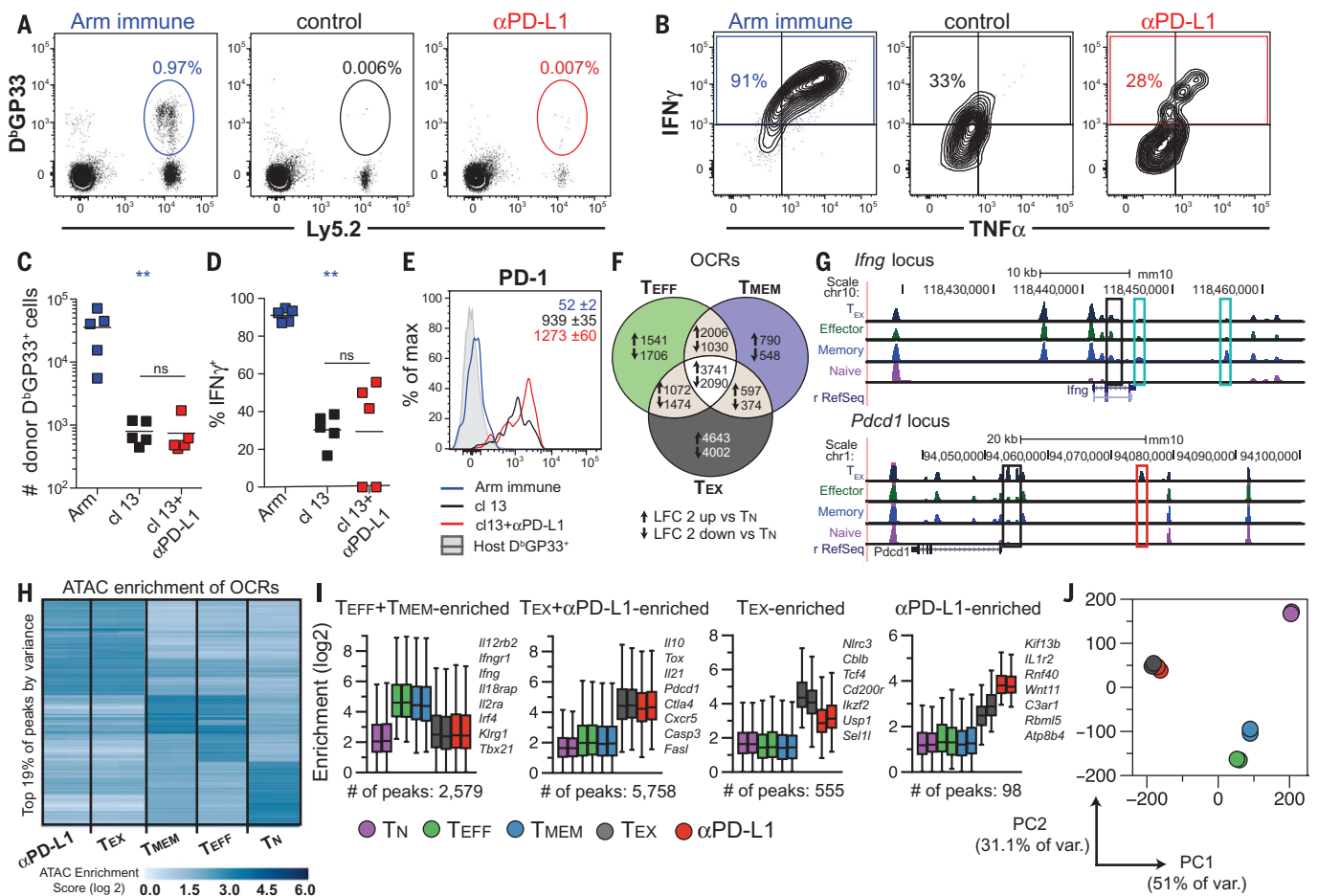


Fig. 3. PD-1 pathway blockade fails to restore memory-like recall capacity or reprogram the epigenetic landscape of T_{EX} into T_{EFF} or T_{MEM} cells.

(A to D) The experimental design outlined in fig. S7A was used except that recipient mice were rechallenged with *Listeria*-GP33 3.5 weeks after transfer. (A) Flow cytometry plots of responding T_{MEM} , T_{EX} , or anti-PD-L1-treated T_{EX} at 6 days after rechallenge with *Listeria*-GP33. (B) Concatenated flow cytometry plots gated on P14 cells from mice in (A) after ex vivo peptide stimulation. (C) Quantification of donor (Ly5.2⁺) D^bGP33⁺ CD8 T cells in the spleens shown in (A). (D) Quantification of IFN γ ⁺ P14 cells shown in (B). (E) Histograms of PD-1 on donor D^bGP33⁺ cells from mice shown in fig. 2B. Values indicate average geometric MFI and SEM. Data are representative of two independent experiments with at least four mice per group. Asterisks indicate statistical significance

(*** $P < 0.01$, and **** $P < 0.001$) determined as described in the supplementary methods. Blue asterisks indicate ANOVA P values; black asterisks indicate post-test P values. (F) Venn diagrams of ATAC-seq OCRs compared to T_N cells (LFC ≥ 2). Data from the two replicates are combined. (G) Representative ATAC-seq tracks from one independent replicate per group shown at the *Ifng* and *Pcdcl1* loci. (H) Cocluster analysis of variance showing enrichment of OCRs in ATAC-seq data set. Solid lines separate cell types, and replicates are shown side by side. (I) Box and whisker plots showing ATAC-seq enrichment from (H). Whiskers represent the interquartile range. (J) Principle-component analysis of all OCRs. For (I) and (J), each replicate is shown. ATAC-seq data are from two independent experiments with 2 to 15 mice per group as described in the supplementary methods.

similarity between control and anti-PD-L1-treated T_{EX} (Fig. 3, H to J, and fig. S11). OCRs preferentially found in both T_{EX} and anti-PD-L1-treated T_{EX} were located near *Pcdcl1*, *Il10*, *Ctla4*, *Cxcr5*, and elsewhere, suggesting state-specific regulation that was not substantially altered after PD-L1 blockade (fig. S13). Although globally, the epigenetic changes were modest, cocluster analysis identified a small subset of OCRs specifically enriched in T_{EX} (555 peaks) or anti-PD-L1-treated T_{EX} (98 peaks) (Fig. 3, H to I; fig. S13; and table S7). Some of these genes showed the same trend epigenetically and transcriptionally (e.g., *CD200r*; fig. S10E), and specific biological pathways were enriched in sets of genes near OCRs that were unique to each cell type. (fig. S15).

T_{EX} displayed ~6000 unique OCR changes compared to T_{EFF} and T_{MEM} (Fig. 3, F to I). Thus, the

~650 OCR changes induced by PD-L1 blockade were modest by comparison. To determine whether these changes affected specific transcriptional circuits, we identified transcription factor (TF) motifs enriched in peaks gained [e.g., nuclear factor κ B (NF- κ B), Jun:AP-1 (activator protein 1), and CCCTC-binding factor (CTCF)] or lost [e.g., nuclear factor of activated T cells, cytoplasmic 1 (NFATc1), NFAT:AP1, Nur77, Eomes, and Egr2] (Fig. 4A). We hypothesized that reinvigoration resulted from rewired transcriptional control within the existing T_{EX} epigenetic landscape. To test this notion, we performed Wellington bootstrap analysis to predict TF binding activity (Fig. 4B and table S10). T_{EX} and anti-PD-L1-treated T_{EX} were more similar to each other than to T_N , T_{EFF} , or T_{MEM} . However, TF motifs biased toward T_{EX} or anti-PD-L1-treated T_{EX} were iden-

tified (Fig. 4B and table S10). TF footprinting was then performed to identify TFs with evidence of likely binding (Fig. 4C and figs. S16 and S17). An integrated network was then constructed for transcriptional circuitry based on predicted TF activity (Fig. 4D and table S11). This network identified augmented activity of NF- κ B, interferon regulatory factors (IRFs), and bZip factors (AP-1 family) and decreased activity of NFAT, Egr2, and Nur77 upon PD-L1 blockade. Major features of this transcriptional network were recapitulated with a second network approach in which additional TF families were identified (e.g., Runx, Nr2f6, Prdm1, Rarb, Pparg, Rxra, and homeobox TFs; fig. S18 and table S12). To further investigate how these changes might affect a specific TF, we examined NFAT. NFAT working with AP-1 transactivates many effector-phase

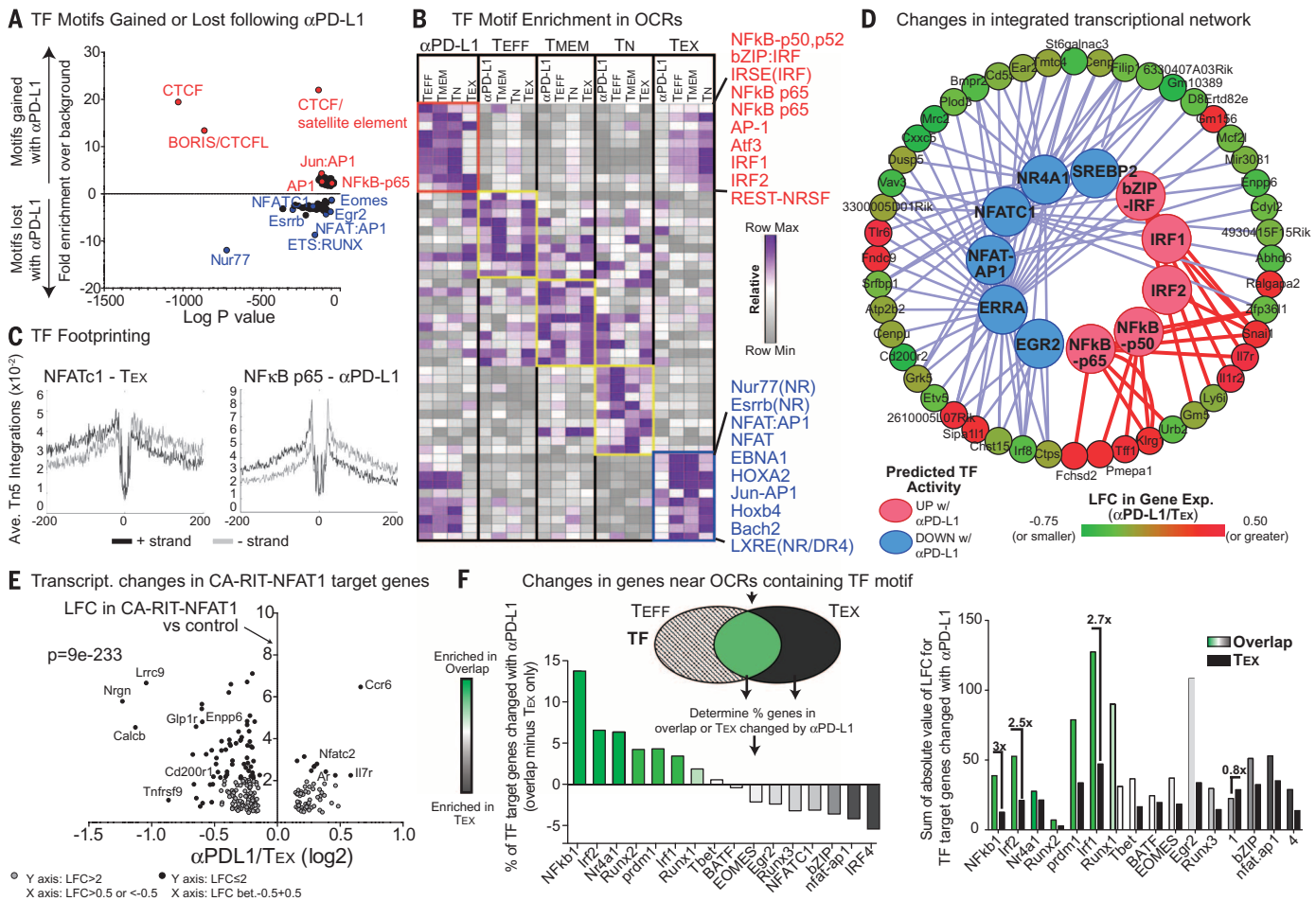


Fig. 4. Differential transcription factor binding after PD-1 pathway blockade contributes to an altered transcriptional network during T_{EX} reinvigoration. (A) Enrichment of TF binding motifs in OCRs lost or gained after anti-PD-L1 treatment. (B) Wellington bootstrap analysis of TF binding in pairwise comparisons for each cell type; the top 10 TFs (in boxes) enriched in all OCRs are shown. Full list in table S10. (C) TF footprint for NFATc1 in T_{EX} and NF- κ B-p65 in anti-PD-L1-treated T_{EX} . (D) Integrated network analysis of the transcriptional and epigenetic changes after anti-PD-L1 treatment. Lines connect TFs predicted to have altered activity to

corresponding genes regulated. Details in table S11. (E) LFC of genes significantly changed by anti-PD-L1 treatment compared to genes significantly induced by the “partnerless” NFAT construct CA-RIT-NFAT1 (30). (F) Venn diagram showing genes near OCRs containing given TF motifs in T_{EFF} , T_{EX} , or both (overlap) (top left). Percentage difference in TF target genes changed ($P < 0.05$, LFC ≥ 0.3) with anti-PD-L1 in overlap compared to T_{EX} only (bottom left). Sum of the absolute value of the LFC in expression in TF target genes after anti-PD-L1 treatment (right). ATAC-seq data shown are combined replicates for each condition.

genes. By contrast, “partnerless” NFAT that fails to bind AP-1 induces a subset of T_{EX} genes (30). Here, upon anti-PD-L1 treatment, there was significantly reduced expression of targets of partnerless NFAT in reinvigorated T_{EX} (Fig. 4E), suggesting a rewiring of this transcriptional circuit after blockade.

Together, these data suggested that, although PD-1 pathway blockade did not fully reprogram T_{EX} into T_{MEM} or T_{EFF} , these cells may (re)acquire some features of T_{EFF} biology. One hypothesis is that upon PD-L1 blockade, the rewired transcriptional network allows T_{EX} to preferentially reengage features of their epigenomic program that overlap with T_{EFF} . To test this idea, we separated TF target genes into those containing OCRs that were (i) specific to T_{EFF} , (ii) specific to T_{EX} , or (iii) shared between T_{EFF} and T_{EX} (Fig. 4F). We then examined the change in genes expressed in each category after PD-L1 blockade. For several TFs, including T-bet and Eomes, there was no redis-

tribution of the pattern of target gene expression (Fig. 4F). However, for many TFs identified above that have a key role in effector biology, such as NF- κ B, IRF1, IRF2, Nur77, and Blimp-1 (encoded by *Prdm1*), there was an increase in the number of target genes expressed in the T_{EFF} and T_{EX} overlap group compared to the T_{EX} -only group upon PD-L1 blockade (Fig. 4F). Moreover, genes in the shared T_{EFF} and T_{EX} epigenetic module displayed a substantially greater magnitude of change in expression than genes in the T_{EX} -only group (Fig. 4F). These data indicate that PD-1 pathway blockade induces rewired transcriptional activity, allowing T_{EX} to more effectively reengage modules of effector genes contained within the epigenetic landscape of T_{EX} . Specific TF circuits that are altered, such as NF- κ B, may have implications for cotargeting PD-1 and TNFR family pathways (1, 3, 31) and may be relevant for the design of future therapeutics.

Our data suggest that in settings of severe T cell exhaustion, reacquiring durable immune memory may be challenging, especially if tumor or viral antigen persists. However, our data also indicate that PD-1 pathway blockade may reveal opportunities to further augment T cell quality or effector activity (e.g., NF- κ B, IL-7R). Additional strategies, such as priming new T cell responses (3), selectively expanding less exhausted subsets (25), or targeting multiple immunoregulatory or homeostatic pathways (e.g., IL-7, IL-2) simultaneously (1, 3), may also augment acquisition of durable immunity. Finally, these studies provide the impetus for extending epigenetic landscape mapping to human T_{EX} , future evaluation of checkpoint blockade combined with epigenetic modifiers, or epigenomic engineering for T cells. Thus, integrated cellular, transcriptional, and epigenetic profiling of T_{EX} not only reveals mechanistic insights into PD-1 pathway blockade-mediated reinvigoration,

but also points to key opportunities for improving the long-term durability of these effects.

REFERENCES AND NOTES

- E. J. Wherry, M. Kurachi, *Nat. Rev. Immunol.* **15**, 486–499 (2015).
- D. B. Page, M. A. Postow, M. K. Callahan, J. P. Allison, J. D. Wolchok, *Annu. Rev. Med.* **65**, 185–202 (2014).
- P. Sharma, J. P. Allison, *Science* **348**, 56–61 (2015).
- D. S. Shin, A. Ribas, *Curr. Opin. Immunol.* **33**, 23–35 (2015).
- D. L. Barber et al., *Nature* **439**, 682–687 (2006).
- See supplementary information on Science Online.
- M. M. Gubin et al., *Nature* **515**, 577–581 (2014).
- B. Bengsch et al., *Immunity* **45**, 358–373 (2016).
- M. M. Staron et al., *Immunity* **41**, 802–814 (2014).
- N. Patsoukis et al., *Sci. Signal.* **5**, ra46 (2012).
- J. Godec et al., *Immunity* **44**, 194–206 (2016).
- H. Shin, S. D. Blackburn, J. N. Blattman, E. J. Wherry, *J. Exp. Med.* **204**, 941–949 (2007).
- E. J. Wherry, D. L. Barber, S. M. Kaech, J. N. Blattman, R. Ahmed, *Proc. Natl. Acad. Sci. U.S.A.* **101**, 16004–16009 (2004).
- M. Pellegrini et al., *Cell* **144**, 601–613 (2011).
- S. G. Nanjappa, E. H. Kim, M. Suresh, *Blood* **117**, 5123–5132 (2011).
- B. Youngblood et al., *Immunity* **35**, 400–412 (2011).
- D. T. Utschneider et al., *Nat. Immunol.* **14**, 603–610 (2013).
- J. M. Angelosanto, S. D. Blackburn, A. Crawford, E. J. Wherry, *J. Virol.* **86**, 8161–8170 (2012).
- F. Zhang et al., *Mol. Ther.* **22**, 1698–1706 (2014).
- J. D. Buenostro, P. G. Giresi, L. C. Zaba, H. Y. Chang, W. J. Greenleaf, *Nat. Methods* **10**, 1213–1218 (2013).
- D. R. Winter, I. Amit, *Immunol. Rev.* **261**, 9–22 (2014).
- K. J. Oestreich, H. Yoon, R. Ahmed, J. M. Boss, *J. Immunol.* **181**, 4832–4839 (2008).
- C. Kao et al., *Nat. Immunol.* **12**, 663–671 (2011).
- M. A. Paley et al., *Science* **338**, 1220–1225 (2012).
- S. D. Blackburn, H. Shin, G. J. Freeman, E. J. Wherry, *Proc. Natl. Acad. Sci. U.S.A.* **105**, 15016–15021 (2008).
- R. He et al., *Nature* **537**, 412–428 (2016).
- S. J. Im et al., *Nature* **537**, 417–421 (2016).
- D. T. Utschneider et al., *Immunity* **45**, 415–427 (2016).
- T. A. Doering et al., *Immunity* **37**, 1130–1144 (2012).
- G. J. Martinez et al., *Immunity* **42**, 265–278 (2015).
- L. K. Ward-Kavanagh, W. W. Lin, J. R. Sedý, C. F. Ware, *Immunity* **44**, 1005–1019 (2016).

ACKNOWLEDGMENTS

We thank the Wherry lab for discussions and critically reading the manuscript. We thank C. Surh for providing the antibody against IL-7 (anti-IL-7). The anti-IL-7 antibody is available from La Jolla Institute of Allergy and Immunology, and the IL-7 used is available from the National Cancer Institute, both under material transfer agreements with the University of Pennsylvania. The data presented in this manuscript are tabulated in the main paper and in the supplementary materials. Sequencing data are available at Gene Expression Omnibus [accession numbers GSE86796 (microarray), GSE86881 (RNA seq), and GSE86797 (ATAC seq)]. This study was supported by a Robertson Foundation–Cancer Research Institute Irvington Fellowship (K.E.P.), an American Cancer Society Postdoctoral Fellowship (M.A.S.), National Institutes of Health grant F30DK100159 (J.M.S.), German Research Foundation Fellowship BE5496/1-1 (B.B.), and National Institutes of Health grant T32 2T32CA009615-26 (A.C.H.). This work was funded by the National Institutes of Health (grant CA78831 to S.L.B. and grants AI105343, AI112521, AI082630, AI115712, AI117950, and AI108545 to E.J.W.). This research was also supported by the Parker Institute for Cancer Immunotherapy. E.J.W. has a patent licensing agreement on the PD-1 pathway. The authors declare no additional conflicts of interest.

SUPPLEMENTARY MATERIALS

www.sciencemag.org/content/354/6316/1160/suppl/DC1

Materials and Methods

Figs. S1 to S18

Tables S1 to S12

References (32–38)

18 January 2016; accepted 19 September 2016

Published online 27 October 2016

10.1126/science.aaf2807

T CELL EXHAUSTION

The epigenetic landscape of T cell exhaustion

Debattama R. Sen,^{1,2*} James Kaminski,^{3*} R. Anthony Barnitz,¹ Makoto Kurachi,^{4,5} Ulrike Gerdemann,¹ Kathleen B. Yates,¹ Hsiao-Wei Tsao,¹ Jernej Godec,^{1,2} Martin W. LaFleur,^{1,2} Flavian D. Brown,^{1,2} Pierre Tonnerre,⁶ Raymond T. Chung,⁶ Damien C. Tully,⁷ Todd M. Allen,⁷ Nicole Frahm,⁸ Georg M. Lauer,⁶ E. John Wherry,^{4,5} Nir Yosef,^{3,7,9††} W. Nicholas Haining^{1,10,11††}

Exhausted T cells in cancer and chronic viral infection express distinctive patterns of genes, including sustained expression of programmed cell death protein 1 (PD-1). However, the regulation of gene expression in exhausted T cells is poorly understood. Here, we define the accessible chromatin landscape in exhausted CD8⁺ T cells and show that it is distinct from functional memory CD8⁺ T cells. Exhausted CD8⁺ T cells in humans and a mouse model of chronic viral infection acquire a state-specific epigenetic landscape organized into functional modules of enhancers. Genome editing shows that PD-1 expression is regulated in part by an exhaustion-specific enhancer that contains essential RAR, T-bet, and Sox3 motifs. Functional enhancer maps may offer targets for genome editing that alter gene expression preferentially in exhausted CD8⁺ T cells.

T cell exhaustion—an acquired state of T cell dysfunction—is a hallmark of cancer and chronic viral infection (1, 2), and clinical trials of checkpoint blockade, which aim to reverse T cell exhaustion in cancer, have proven strikingly effective (3, 4). Chimeric antigen receptor (CAR)-T cell therapy has also proven highly effective for hematologic malignancies (5), but the development of exhaustion in T cells engineered to treat solid tumors remains a substantial barrier to its broader use (6). The identification of mechanisms that regulate exhausted T cells is therefore a major goal in cancer immunotherapy.

To identify regulatory regions in the genome of exhausted CD8⁺ T cells, we used an assay for transposase-accessible chromatin with high-throughput sequencing (ATAC-seq) (7) to demarcate areas of accessible chromatin in mouse

antigen-specific CD8⁺ T cells differentiating in response to lymphocytic choriomeningitis virus (LCMV) infection (fig. S1A and table S1). Acute LCMV infection elicits highly functional effector CD8⁺ T cells, whereas chronic LCMV infection gives rise to exhausted CD8⁺ T cells (1–3, 8, 9). Analysis of high-quality ATAC-seq profiles (fig. S1, B to H) from naïve CD8⁺ T cells and those at day 8 and day 27 postinfection (p.i.) (d8 and d27, respectively) revealed that naïve CD8⁺ T cells underwent large-scale remodeling (Fig. 1A and fig. S2A) during differentiation [as detected by DESeq2, with a false discovery rate (FDR) < 0.05]. The majority (71%) (fig. S2A) of chromatin-accessible regions (ChARs) either emerged (e.g., those at the *Ifng* locus) or disappeared (e.g., *Ccr7*) (Fig. 1A) as naïve CD8⁺ T cells underwent differentiation. The gain and loss of ChARs were not balanced; a much larger fraction of regions emerged at d8 p.i. and persisted or emerged only at d27 than were either transiently detected at d8 p.i. or lost from naïve cells (Fig. 1B). Thus, differentiation from a naïve CD8⁺ T cell state is associated with a net increase, rather than decrease, in chromatin accessibility (fig. S2B).

Comparison of ChARs from exhausted CD8⁺ T cells with those found in functional effector or memory CD8⁺ T cells revealed marked differences in the pattern of regulatory regions. Differential regulatory regions between acute and chronic infection (Fig. 1C and fig. S2C) showed features of enhancers: They tended to be depleted of transcription start sites (TSSs) and enriched for intergenic and intronic areas (Fig. 1D), and found distal to gene promoters (fig. S2D). The magnitude of difference in the profile of regulatory regions between exhausted and functional CD8⁺ T cells was greater than that seen in gene expression. We found that 44.48% of all ChARs

¹Department of Pediatric Oncology, Dana-Farber Cancer Institute, Boston, MA 02115, USA. ²Division of Medical Sciences, Harvard Medical School, Boston, MA 02115, USA.

³Center for Computational Biology, University of California, Berkeley, Berkeley, CA 94720, USA. ⁴Institute of Immunology, University of Pennsylvania, Philadelphia, PA 19104, USA. ⁵Department of Microbiology, University of Pennsylvania, Philadelphia, PA 19104, USA. ⁶Gastrointestinal Unit and Liver Center, Massachusetts General Hospital, Harvard Medical School, Boston, MA 02115, USA. ⁷Ragon Institute of Massachusetts General Hospital, Massachusetts Institute of Technology, and Harvard University, Boston, MA 02139, USA. ⁸Vaccine and Infectious Disease Division, Fred Hutchinson Cancer Research Center, Seattle, WA 98109, USA. ⁹Department of Electrical Engineering and Computer Science, University of California, Berkeley, Berkeley, CA 94720, USA. ¹⁰Division of Pediatric Hematology and Oncology, Children's Hospital, Boston, MA 02115, USA. ¹¹Broad Institute of Harvard and Massachusetts Institute of Technology, Cambridge, MA 02142, USA.

*These authors contributed equally to this work. †These authors contributed equally to this work. ††Corresponding author. Email: nir.yosef@berkeley.edu (N.Y.); nicholas_haining@dfci.harvard.edu (W.N.H.)



Epigenetic stability of exhausted T cells limits durability of reinvigoration by PD-1 blockade

Kristen E. Pauken, Morgan A. Sammons, Pamela M. Odorizzi, Sasikanth Manne, Jernej Godec, Omar Khan, Adam M. Drake, Zeyu Chen, Debattama R. Sen, Makoto Kurachi, R. Anthony Barnitz, Caroline Bartman, Bertram Bengsch, Alexander C. Huang, Jason M. Schenkel, Golnaz Vahedi, W. Nicholas Haining, Shelley L. Berger and E. John Wherry (October 27, 2016)
Science **354** (6316), 1160-1165. [doi: 10.1126/science.aaf2807]
originally published online October 27, 2016

Editor's Summary

The epigenetics of exhaustion

During cancer or chronic infection, T cells become dysfunctional, eventually acquiring an "exhausted" phenotype. Immunotherapies aim to reverse this state. Using a mouse model of chronic infection, two studies now show that the epigenetic profile of exhausted T cells differs substantially from those of effector and memory T cells, suggesting that exhausted T cells are a distinct lineage (see the Perspective by Turner and Russ). Sen *et al.* defined specific functional modules of enhancers that are also conserved in exhausted human T cells. Pauken *et al.* examined the epigenetic profile of exhausted T cells after immunotherapy. Although there was transcriptional rewiring, the cells never acquired a memory T cell phenotype. Thus, epigenetic regulation may limit the success of immunotherapies.

Science, this issue p. 1104, p. 1165; see also p. 1160

This copy is for your personal, non-commercial use only.

- Article Tools** Visit the online version of this article to access the personalization and article tools:
<http://science.sciencemag.org/content/354/6316/1160>
- Permissions** Obtain information about reproducing this article:
<http://www.sciencemag.org/about/permissions.dtl>

Science (print ISSN 0036-8075; online ISSN 1095-9203) is published weekly, except the last week in December, by the American Association for the Advancement of Science, 1200 New York Avenue NW, Washington, DC 20005. Copyright 2016 by the American Association for the Advancement of Science; all rights reserved. The title *Science* is a registered trademark of AAAS.